RSC Applied Polymers

ROYAL SOCIETY OF CHEMISTRY

PAPER

View Article Online
View Journal | View Issue

Cite this: *RSC Appl. Polym.*, 2024, **2**, 1124

Fluorescent histidine-derived biodynamers as biocompatible and highly water-soluble copper(II)-sensors†

Lena Zeroug-Metz,[a] Mohamed A. M. Kamal,[b] Justine Bassil,[b] Kalanika Elamaldeniya,[c] Bo Hyun Ryu,[c] Eric Buhler[d] and Sangeun Lee *[a,b]

Amino-acid derived biodynamers, characterized as dynamic biopolymers, are synthesized under acidic pH conditions through dynamic covalent chemistry (DCC) between amino acid hydrazides and carbazole hexaethylene glycols (CA-HG). In the field of biomedical research, especially for the designs of smart drug delivery systems, DCC has increasingly gained popularity within the last years. Biodynamers possess a range of advantageous properties, such as fluorescence, tunability through amino acid monomer exchange, water solubility, and biocompatibility. These characteristics make them promising materials for a variety of biomedical applications. By leveraging these beneficial traits, biodynamers can be applied as detectors for physiologically important metal ions, utilizing changes in their fluorescence emission upon binding to the DCC framework and polymer's side chains. In this study, we investigated the potential of histidine-based biodynamers (HisBD) for detecting a key biomarker, Cu(II), using *in silico* simulations and cuvette assays. Our results revealed that HisBD exhibited selective fluorescence in the presence of Cu(II), with approximately 90% quenching of fluorescence due to binding site interactions and side chain effects under physiological conditions. This study broadens the applications of DCC and underscores the potential of HisBD as a candidate for Cu(II) chemosensors, overcoming the limitations of current systems such as limited solubility, sensitivity, and biocompatibility.

Received 5th April 2024,
Accepted 5th September 2024

DOI: 10.1039/d4lp00126e

rsc.li/rscapplpolym

Introduction

Dynamic covalent chemistry (DCC), which merges the dynamic principles of supramolecular chemistry into covalent chemistry on the molecular level, has progressively gained prominence within the field of chemistry in recent decades.[1–3] While supramolecular chemistry predominantly relies on non-covalent interactions, DCC expands to the reversible formation and cleavage of covalent bonds within/between molecules.[4–7] This discipline significantly impacts polymer science by enabling post-formation adjustments to product distributions through changes in temperature, concentration, and pH, thereby facilitating the development of dynamic covalent polymers, or dynamers.[8,9]

These dynamers possess favorable properties such as malleability, self-healing capabilities, and customizable mechanical traits, rendering them valuable across diverse applications ranging from materials science to biomedicine.[10] The applicability of dynamers, especially dynamic biopolymers, for drug and protein delivery as well as antibacterial potentiators has gained increasing attention within recent years.[11–14] However, the exploration of their potential as ion-recognition molecules and chemosensors in medicine remains underexplored. Considering the reversibility of dynamers and the incorporation of adjustable functional groups like fluorophores and chelating moieties, they may offer promising prospects for their utilization as ion-chemosensors and, in general, biosensing.[15–17]

Proteoid dynamic biopolymers, known as biodynamers, are a class of biopolymers synthesized through the principles of DCC, wherein reversible covalent bonds form between amino acid hydrazides and carbazole hexaethylene glycols (CA-HG).[1,18,19] Our previous studies have revealed several noteworthy features of biodynamers. Firstly, they demonstrate fluorescence attributed to CA-HG emission and exhibit pH-responsive degradation facilitated by DCC. While biodynamers

[a]*Pharmaceutical Materials and Processing, Department of Pharmacy, Saarland University, Campus C4. 1, 66123 Saarbrücken, Germany.*
E-mail: sangeun.lee@uni-saarland.de
[b]*Helmholtz Institute of Pharmaceutical Research Saarland (HIPS) – Helmholtz Centre for Infection Research (HZI), Campus E8.1, 66123 Saarbrücken, Germany*
[c]*Korea Institute of Science and Technology Europe, Forschungsgesellschaft mbH, Campus E7.1, 66123 Saarbrücken, Germany*
[d]*Laboratoire Matière et Systèmes Complexes (MSC), UMR CNRS 7057, Université Paris Cité, Physics Department, Bâtiment Condorcet, 75013 Paris, France*
† Electronic supplementary information (ESI) available. See DOI: https://doi.org/10.1039/d4lp00126e

exhibit degradation in physiological acidic environments, such as those found in inflammation and tumor sites, they remain stable under neutral and basic conditions. Despite the intrinsic dynamic nature of their functional groups, including imines and acylhydrazones, the hydrophobic core derived from CA significantly enhances their overall stability.[18,20] Secondly, biodynamers are easily modifiable by incorporating various amino acid monomer compositions.[18] Third, the resulting biodynamers self-organize into nanorod-like or globular structures driven by the encapsulation of hydrophilic HG chains as well as hydrophobic interactions along with π–π stacking between aromatic CA rings, resulting in remarkable water solubility and biocompatibility.[8,21] As an example, Lysine-derived biodynamers (LysBDs) displayed a 44-fold lower toxicity than the widely known poly-L-lysine.[11] These advantages enabled us to explore the potential of biodynamers as pH-responsive drug-delivery systems for nucleic acids and proteins.[11]

Focusing on the fluorescent traits and functional groups, biodynamers possess favorable attributes for metal ion detection. Firstly, the presence of acylhydrazones and imines within the biodynamers' backbone are known as ion binding sites.[16,17,20,22] Secondly, the fluorescence exhibited by CA offers a direct indicator of ion binding.[23–25] Last but not least, amino acid side chains, such as histidine residues, demonstrate a pronounced affinity towards Cu(II) ions, presenting additional binding sites for the targeted ions (Scheme 1).[26–29]

As one of the major trace elements found in the human body, Cu(II) serves several important functions, including acting as a catalyst for enzyme redox chemistry, scavenging free radicals, and aiding in mitochondrial respiration.[30–33] While Cu(II) is necessary for various vital physiological processes, minor disruptions in its concentration have severe consequences for one's health, leading to the development of neurological diseases like Alzheimer's and Wilson's disease, as well as contributing to tumor progression.[34–36] Furthermore, due to its environmental impact, Cu(II) is classified as a hazardous heavy metal.[37] Ingestion through drinking water in concentrations >20 μM poses substantial acute and chronic risks to the human body.[38] Therefore, efficient and highly accurate monitoring of Cu(II) levels is essential for both environmental and medical purposes. Current and widely used methods for detecting metal ions in low concentrations, such as atomic absorption spectroscopy (AAS) or inductively coupled plasma mass spectroscopy (ICP-MS), are both costly and destructive to the reporter molecule.[39–41]

As promising alternatives, fluorescent organic molecule-based chelators have emerged as highly efficient, fast and non-destructive ion-chemosensors.[22,25,42–45] Recent designs of Cu(II) sensors include imine-rich Schiff bases, fluorescein, salicylhydrazones, and BODIPY-based compounds, which have become valuable agents for Cu(II) detection.[46–49] Interactions between the metal ion and the coordinating sites of the fluorophore enable the sensors to either exhibit an on–off (ion-dependent quenching) or off-on (ion-dependent fluorescence) response, facilitating rapid and highly reproducible quantification of metal ions.[50–52] Despite their many advantages, fluorescent, small organic molecule-based chelators often possess limited solubility and/or ion-sensitivity in aqueous, physiological medium, rendering them less desirable for Cu(II) detection for biological applications.

As an approach to overcoming the limitation of water compatibility, the focus has shifted towards developing more water-soluble sensors for Cu(II), extending the system from molecules to nanoparticles and polymers. In the case of Wang *et al.*, an on–off water-soluble fluorescent tetradentate ligand, (BIP), for Cu(II) recognition was designed.[53] This Cu(II) sensor demonstrated high sensitivity and selectivity for Cu(II) detec-

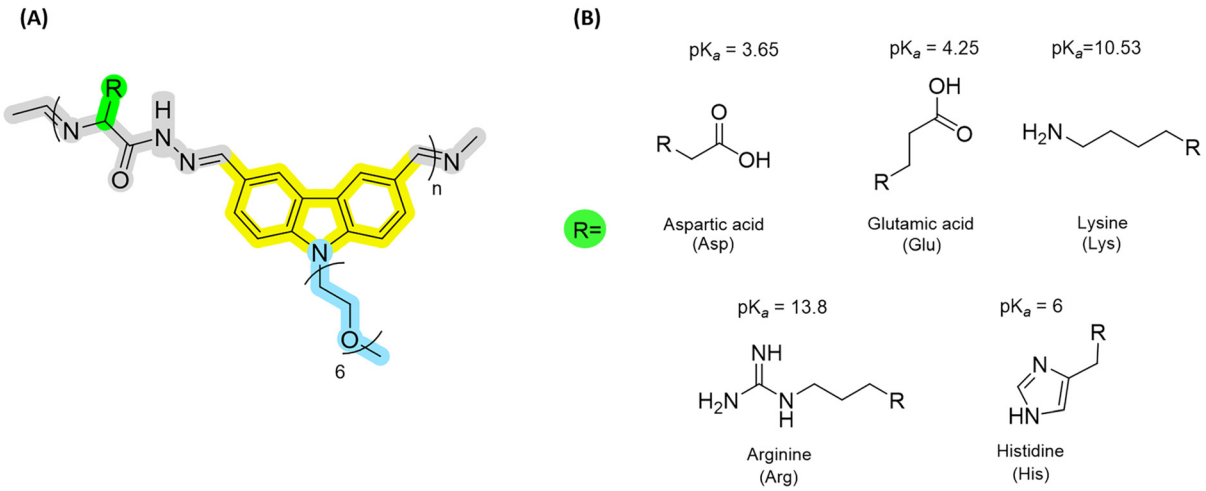

Scheme 1 Chemical structure of (A) the repeating unit (dimer) of biodynamers, containing reversible imine and acylhydrazone bonds (grey), amino acid-derived side chains (green), carbazole dialdehyde as fluorophore (yellow) and a hexaethylene glycol chain (blue). (B) displays the different proteoid side chains (R) with corresponding pK_a-values.

tion in aqueous solutions, highlighting its potential for environmental research applications. Another recent publication by Çimen *et al.* reviewed the application of nanomaterial-based plasmonic nanosensors for detecting water pollutants.[38] Here, the advantages of using *e.g.* gold nanoparticles and quantum dots as ion-sensors with high sensitivity and selectivity for trace pollutants such as toxins, bacteria, and heavy metals were investigated. Sun *et al.* presented another approach by designing a water-soluble polymer probe, PEG-R, which integrates polyethylene glycol into the rhodamine platform.[54] This probe exhibited rapid and efficient Cu(II) detection, responding within 30 seconds and achieving approximately 29-fold fluorescence enhancement. PEG-R demonstrated high selectivity and sensitivity for Cu(II) detection *in vivo* and *in vitro*, overcoming the common issue of limited water solubility and ion-selectivity. As discussed by Choudhury *et al.*, current polymeric sensors incorporate pendant metal-ion-recognition motifs, integrating specific metal-ion recognition units into the polymer matrix.[55] This platform detects specific metal ions by leveraging their binding interactions with organic ligands, resulting in noticeable fluorometric changes.

When focusing on Cu(II) detectors for medical and diagnostic purposes, enhanced cytotoxicity is a critical issue when applied to living biological systems. As reported by Hu *et al.*, a stimuli-responsive polymeric material providing good water solubility and biocompatibility was developed. These features make them suitable for detecting and capturing toxic metal ions in both water and cellular environments.[56] Despite advancements in Cu(II) sensor designs, challenges related to biocompatibility and ion selectivity create a strong incentive to further expand and optimize the design of dynamic, polymeric Cu(II) sensors.

In this study, we investigated fluorescent, histidine-derived biodynamers (HisBD) as Cu(II)-sensing agents *via* ion-induced quenching for diagnostic applications. Our approach involved evaluating the Cu(II) binding potential of HisBD through *in silico* models, as well as in cuvette and *in vitro* experiments. We found that HisBD exhibits a reversible, ion-selective and sensitive affinity towards Cu(II) under physiological conditions and confirmed their biocompatibility. Additionally, we explored the role of functional groups in HisBD for ion coordination, emphasizing the importance of DCC and sidechain-specificity for ion selectivity.

Experimental section

Chemicals

Copper(II) sulfate pentahydrate ($CuSO_4{\cdot}5H_2O$, 99%) was purchased by Geyer Th. GmbH & Co. KG. Sodium chloride (NaCl) was purchased from BDH Prolabo, potassium chloride (KCl), magnesium chloride ($MgCl_2$), calcium chloride dihydrate ($CaCl_2{\cdot}2H_2O$), cobalt(II) nitrate hexahydrate (Co $(NO_3)_2{\cdot}6H_2O$) and disodium ethylenediaminetetraacetate dihydrate ($EDTANa_2{\cdot}2H_2O$) were purchased from Sigma-Aldrich. Iron(III) chloride ($FeCl_3$), iron(II) sulfate heptahydrate ($FeSO_4{\cdot}7H_2O$) and zinc(II) ($ZnCl_2$) were also purchased from Sigma-Aldrich.

Stated purities, forms, and sources are specific to the materials used in this study and may vary for various sources or batches. All chemicals were used as purchased without any further purification.

In silico simulation *via* AutoDock Vina MD

The molecular docking (MD) modelling was performed to investigate the interaction, namely, specific binding mode, sites and free energy of Cu(II) with a target molecule (HisBD). Here the software AutoDock Vina (v1.2.0) and AutoDock Tools (v1.5.7) were used. The Lamarckian genetic algorithm was implemented to determine the preferred binding sites on the target molecule with Cu(II). The molecular modelling output from AutoDock Vina (v1.2.0) was further analyzed *via* Discovery Studio (v1.3) to identify the most preferable interaction between Cu(II) and the target molecule (HisBD). The reliability of molecular modeling outcomes was assessed by evaluating RMSD (root mean square deviation) values. This is based on the fact that lower RMSD values serve as an indication that the predicted binding conformation closely aligns with the actual structure, thereby enhancing confidence in the accuracy of the predictions. Combining a low RMSD and accurate free energy predictions provides strong evidence for the reliability of the molecular modeling study.

Synthesis of amino acid-derived biodynamers

The amino acid-derived biodynamers were synthesized following an established protocol by Liu *et al.* Here, CA-HG and amino acid hydrazide were combined in a 1 : 1 molar ratio in a 10 mM acetic acid solution under mildly acidic conditions. The reaction proceeded for 24 hours at room temperature with exclusion of light (see Scheme S1†). As described in our previous papers, the completion of polymerization is confirmed using ^{1}H-NMR spectroscopy.[21] In our study, the NMR analysis of HisBD was performed on the AVANCE III 500 MHz spectrometer. For this, histidine-hydrazide and CA-HG were prepared in deuterated acetic acid solution (10 mM). After combining both monomer solutions in a 1 : 1 molar ratio, a 10 mM polymer solution was obtained. The NMR-spectra were measured 10 minutes (Fig. S1(A)†) and 24 hours (Fig. S1(B)†) after starting the polymerization reaction.

Light scattering analysis

The measurements used a 3D light scattering spectrometer (LS Instruments, Fribourg, Switzerland) equipped with a 120 mW single frequency collimated laser module (Ondax laser diode) operating at λ = 638 nm and coupled to a single mode fiber (with a 4 mm germanium doped core fused with a 125 mm silica cladding, OZ Optics Ltd, Canada), a two-channel multiple tau correlator (1088 channels in autocorrelation), a variable-angle detection system, and a temperature-controlled index matching vat (LS Instruments). The scattering spectrum was measured using two single-mode fiber detections and two

high sensitivity APD detectors (Excelitas Technologies, model SPCM-AQR-13-FC).

Fluctuations in the scattered intensity with time $I(q,t)$ (also called count rate), measured at a given scattering angle θ or equivalently at a given scattering wave vector $q = (4\pi n/\lambda)\sin(\theta/2)$ are directly reflecting the so-called Brownian motion of the scattering particles. In dynamic light scattering (DLS), the fluctuation pattern is translated into the normalized time autocorrelation function of the scattered intensity, $g^{(2)}(q,t)$ defined as:

$$g^{(2)}(q,t) = \frac{\langle I(q,0)I(q,t)\rangle}{\langle I(q,0)\rangle^2} \quad (1)$$

It is related to the so-called dynamic structure factor (or concentration fluctuations autocorrelation function), $g^{(1)}(q,t)$, *via* the Siegert relation:

$$g^{(2)}(q,t) - 1 = \beta|g^{(1)}(q,t)|^2 \quad (2)$$

where β is the coherence factor, which in our experiments is varying between 0.60 and 0.80, depending on the samples and the concentration. The normalized dynamical correlation function, $g^{(1)}(q,t)$, of concentration fluctuations is defined as:

$$g^{(1)}(q,t) = \frac{\langle \delta c(q,0)\delta c(q,t)\rangle}{\langle \delta c(q,0)^2\rangle} \quad (3)$$

where $\delta c(q,t)$ and $\delta c(q,0)$ represent fluctuations of the concentration at time t and zero, respectively. The distribution of decay rates $G(\Gamma)$ was determined using the CONTIN algorithm based on the inverse Laplace transform of $g^{(1)}(q,t)$:

$$g^{(1)}(q,t) = \int_0^\infty G(\Gamma)\exp(-\Gamma t)\mathrm{d}\Gamma \quad (4)$$

For a diffusive process, with characteristic time, $\tau = 1/\Gamma$, inversely proportioned to q^2, $g^{(1)}(q,t) \sim \exp(-Dq^2t)$, with D the mutual diffusion coefficient. The Stokes–Einstein relation allows one to determine the hydrodynamic radius R_h of the scattered objects; $R_h = kT/6\pi\eta D$, or the hydrodynamic diameter, $D_h = kT/3\pi\eta D$, if the temperature T and solvent viscosity η are known (here η = 1.002 cP at 20 °C for water). In our experiments, solutions were characterized by a single relaxation mechanism. We then also adopted the cumulant analysis:

$$\ln g^{(1)}(q,t) = k_0 - k_1 t + \frac{k_2}{2}t^2 + \ldots \quad (5)$$

where $k_1 = 1/\langle\tau\rangle$ and $k_2/{k_1}^2$ represents the polydispersity index. The extrapolation of $(\langle\tau\rangle q^2)^{-1}$ to $q = 0$ yields the mutual diffusion coefficient D.

In static light scattering (SLS) experiments, the excess of scattered intensity is measured with respect to the solvent. The so-called excess Rayleigh ratio of biodynamers was deduced using a toluene sample reference for which the unpolarized excess Rayleigh ratio is well-known ($R_{u,\ toluene} = 10.3 \times 10^{-6}$ cm^{-1} at 633 nm and $\theta = 90°$ if the incident laser beam is depolarized by the non-polarization maintaining fiber):

$$R_{u,\,biodynamers}(q)(cm^{-1}) = \frac{I_{solution}(q) - I_{solvent}(q)}{I_{toluene\ at\ 90°}} \times \left(\frac{n}{n_{toluene}}\right)^2 \times R_{u,\,toluene\ at\ 90°}(cm^{-1}) \quad (6)$$

The dark count (<1 kHz) was subtracted from each intensity measurement. The usual equation for absolute light scattering combines the form factor $P(q)$, the structure factor $S(q)$, and the weight-averaged molecular weight M_w of the scattered objects:

$$\frac{R_u(q)}{1+\cos^2\theta} = \frac{2\pi^2 n^2}{N_a\lambda^4}\left(\frac{\mathrm{d}n}{\mathrm{d}c}\right)^2 cM_wP(q)S(q) \quad (7)$$

where $K^* = 2\pi^2n^2(\mathrm{d}n/\mathrm{d}c)^2/N_A\lambda^4 = 1.20 \times 10^{-7}$ cm^2 g^{-2} mol is the scattering constant in the case of unpolarized incident light (refractive index n = 1.33 for water solvent at 20 °C), c the concentration in g cm^{-3}, and N_a the Avogadro's number. A refractive index increment of $\mathrm{d}n/\mathrm{d}c$ = 0.185 cm^3 g^{-1} determined previously for similar molecules was considered to be a sufficient approximation. The extrapolation of the Rayleigh ratio to zero-q, with $P(q = 0) = 1$ and $S(q) \sim 1$ (*i.e.*, neglecting virial effects in dilute regime), allows determination of M_w and thus of biodynamer's degree of polymerization (DP).

Stability study

A 10 mM HisBD solution was prepared using 10 mM phosphate buffer (pH 7.4) as solvent (see Fig. S2†). The analysis was performed *via* dynamic light scattering (DLS) using a Zetasizer Ultra (Malvern Panalytical, Malvern, UK). Throughout the experiment, the samples were protected from light and stored at room temperature. The parameters measured included the *Z*-Average and polydispersity index (PDI). The experiment was conducted in triplicate (n = 3) with 3 individual HisBD samples, leading to 9 measurements in total.

Preparation of ion-biodynamer complexes

Lysine-biodynamer (LysBD), Arginine-biodynamer (ArgBD), Phenylalanine-biodynamer (PheBD), Aspartic acid-biodynamer (AspBD), Glutamic acid-biodynamer (GluBD) and Histidine-biodynamer (HisBD) were lyophilized and subsequently utilized for each experiment. The biodynamers were dissolved (100 μM) in 200 μL of 10 mM phosphate buffer (pH 7.4) and placed in a well of a 96-well Greiner UV-star well plate. The emission measurements were performed by a TecanReader® Infinite M200 microplate spectrophotometer (Tecan, Männedorf, Switzerland). Each metal ion was added in a concentration of 50 μM (1 : 2 ratio metal to biodynamer) to the biodynamers solutions. The fluorescence intensity was evaluated based on the biodynamers' maxima (see Table S1†). For HisBD, the fluorescence was measured at 525 nm. In addition, emission measurements were conducted for each biodynamer at a concentration of 100 μM without the addition of any metal ions, representing the value of 100% relative fluo-

rescence intensity. The experiment was conducted in triplicate (n = 3).

Molecular weight analysis

The molecular weight (M_w) of HisBD upon the introduction of Cu(II) was analyzed using static light scattering (SLS) using a Zetasizer Ultra (Malvern Panalytical, Malvern, UK). Two dilution series of HisBD in a pH 7.4 phosphate buffer solution (10 mM) were prepared, with concentrations ranging from 15, 10, 7.5, down to 2.5 mM, and subsequently analyzed. For the samples containing Cu(II), 0.5 molar equivalents of the ion were added to each dilution of HisBD. The M_w of both samples (with and without Cu(II)) was determined through static Debye plot analysis and subsequently compared (see Fig. S3†). The experiment was performed in triplicate (n = 3).

In silico simulation *via* molecular operating environment (MOE)

The *in silico* experiment was conducted by the software Molecular Operating Environment (MOE) version 2020. The software underwent conformational search using stochastic search (all default settings were used except for the rejection limit, which was set at 1000). For each experiment and simulation, 5 repeating units of HisBD were added and calculated together with Cu(II). The best conformer was reused and then plotted once again on the MOE, then another stochastic search was done by using a low MD setting (default setting was used except for the rejection limit, which was set at 1000). The HG-chains of HisBD were omitted for the simulation to reduce computing time.

Competing Cu(II)-chelator experiment

Disodium ethylenediaminetetraacetate dihydrate (EDTA-Na_2·$2H_2O$) was dissolved in 10 mM phosphate buffer (pH 7.4) and then added to a previously prepared solution of HisBD (100 μM) and 50 μM Cu(II). After the measurement of the fluorescence intensity at the maximum of 525 nm after the Cu(II) induced quenching, the fluorescence between each titration step of EDTA-Na_2 addition was measured *via* the Tecan reader spectrometer (Model Infinite® M1000). The excitation wavelength was adjusted to 310 nm. To visualize the fluorescence recovery, all samples were prepared after the same protocol to a final volume of 2 mL in a plastic acryl cuvette. An UV-lamp with an excitation of 365 nm was applied. This experiment was performed in triplicates to ensure reproducibility (n = 3).

Biocompatibility *via* MTT-assay

Using A549 epithelial adenocarcinoma cell line, a cell-toxicity evaluation with histidine, lysine- and arginine biodynamer (HisBD, LysBD and ArgBD, respectively) was conducted. The A549 cells (ATCC ACL107) were obtained from the DSMZ (Braunschweig, Germany). The cell viability was measured using a 3-(4,5-dimethylthiazol-2-yl)-2,5-diphenyltetrazolium-bromid (MTT)-assay. Under sterile conditions, 2.0×10^4 cells per well were seeded into a 96-well plate. For each sample and concentration, 3 wells in total were treated for 24 h and 48 h in 37 °C and 5% of CO_2. The range of polymer concentrations was chosen based on previous MTT assays and included 31.25, 62.5, 125, 250, and 500 μg mL^{-1}. After 24 or 48 hours of incubation, the treatment was removed. Subsequently, 10% MTT agent was added to each well and incubated for 4 hours. Following the aspiration of the MTT agent, formazan crystals formed in the presence of viable cells. DMSO was then added, and the well plate was gently shaken for 20 minutes during incubation. After 20 minutes, the absorption of each well was measured at a wavelength of 550 nm. For the negative control, cells were treated with FCS supplemented RPMI cell medium alone, while Triton X (2%) was used for the positive control. The 24-hour and 48-hour MTT assays were performed separately and conducted in triplicates to ensure reproducibility (n = 3).

Results and discussion

In silico simulation of Cu(II)-binding sites on HisBD

In recent years, computational molecular models have been used for reliable prediction of non-covalent interactions such as ligand-to-ion coordination.[57–59] To begin our study, we evaluated the coordination affinity of functional groups in amino-acid derived biodynamers towards Cu(II) by performing an *in silico* simulation using the AutoDock Vina MD software. As previously reported, nitrogen- and oxygen-rich functional groups such as imines, acylhydrazones and imidazoles have been identified as potential coordination sites for metal ions like Cu(II).[17,46,53] Therefore, we simulated the interaction attributes of Cu(II) with a segment (trimer) of HisBD, composed of two histidine-hydrazide units and one CA-HG unit, to evaluate the potential affinity of Cu(II) towards the biodynamer's backbone and chromophore (imines and acylhydrazone bonds) as well as the side chain (histidine). The calculated values of the specified parameters in this simulation indicate the likelihood of achieving accurate polymer-to-metal ion docking outcomes by predicting the binding affinity. These parameters include the free binding energy (kcal mol^{-1}) and the distance or bond length between the metal ion and the binding atoms (Å).

Evaluating the results of this experiment, the most favorable binding sites for Cu(II) were found to be the imine bonds, which are integral components of both the biodynamers' backbone and fluorophore (Fig. 1A). The lowest energy state through a binding affinity was calculated with a binding free energy of −0.7 kcal mol^{-1}, with Cu(II) positioned at a distance of 2.46 Å to O27 and 2.45 Å to N18 of the respective imine within HisBD. The second most probable binding site of the simulation was observed at the heteroatoms constituting elements within the acylhydrazone moiety (Fig. 1B), displaying a binding free energy of −0.6 kcal mol^{-1}. The calculated distances between the Cu(II) and the respective binding atoms of acylhydrazone, O23 and N20, showed values of 2.56 and 2.59 Å, respectively.

As shown in previous studies, our results suggest potential coordination sites for Cu(II) in HisBD by demonstrating the lowest free binding energy for the experimental setup.[60]

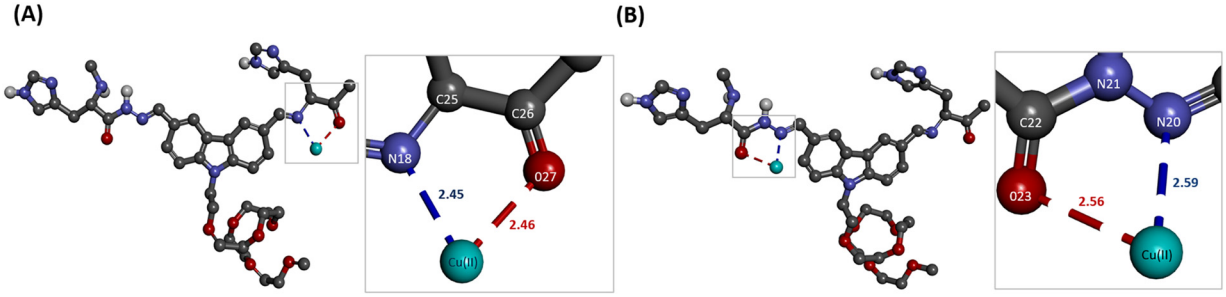

Fig. 1 Molecular dynamics (MD) AutoDock Vina *in silico* simulation of a biodynamer trimer (two units of amino acid side chains and one carbazole-hexaethylene glycol moiety) and the Cu(II)-binding site with the numbered heteroatoms involved. The calculated binding-distances are displayed in Angstrom (Å): (A) most preferable and probable binding mode with Cu(II) to imine interaction. (B) Second to most preferable and probable binding mode showing Cu(II) affinity towards acylhydrazone. Nitrogen is displayed in red, oxygen in blue and Cu(II) in turquoise, respectively.

Although the HisBD was chosen for this experiment, the impact of the imidazole side chain has not yet been confirmed. However, the results from the AutoDock Vina *in silico* simulations present two potential scenarios. First, they imply a plausible interaction between Cu(II) and the dynamic covalent functional groups, imine and acylhydrazone, by calculating the lowest binding free energy. Second, they suggest the potential to induce Cu(II)-dependent fluorescence changes, as the most favorable binding sites identified in this experiment are part of the biodynamer's chromophore.

Characterization of amino acid-derived biodynamers

Building on the promising results from the first *in silico* simulation, we synthesized five amino acid-derived biodynamers, proceeding with in cuvette experiments. In addition to HisBD, four additional biodynamers were selected for this study: lysine-biodynamers (LysBD), arginine-biodynamers (ArgBD), aspartic acid-biodynamers (AspBD), and glutamic acid-biodynamers (GluBD) (see Scheme S1†).[21] As previously reported, the respective biodynamers have already been extensively characterized.[8,13,14,20] Building on this data, we conducted additional characterizations of the polymers. To verify the success of our synthesis, we analyzed the ^{1}H-NMR spectrum of HisBD at the start (0 h) and end of the synthesis (24 h). As shown in Fig. S2,† the aldehyde peak at 9.45 ppm from the CA-HG is clearly present int the spectrum at 0 hours after the initiation of the synthesis. After 24 hours, however, the completion of polymerization is evidenced by the disappearance of the aldehyde peak on the CA moiety, aligning with previous results.[21] Furthermore, as exemplified by HisBD, we confirmed the change in the absorption and emission spectra compared to the fluorescent monomer CA-HG (see Fig. S4†).

Using dynamic light scattering (DLS) and static light scattering (SLS) analyses, the hydrodynamic diameters (D_H) and molar masses of the respective biodynamers were determined (Fig. 2, Fig. S5A–D†). The D_H and molar masses of the prepared biodynamers were determined using DLS and SLS, respectively (Fig. 2, Fig. S5A–D†). The correlation function is characterized by a single diffusive exponential decay with a main characteristic relaxation time varying as $\tau \sim q^{-2}$ allowing

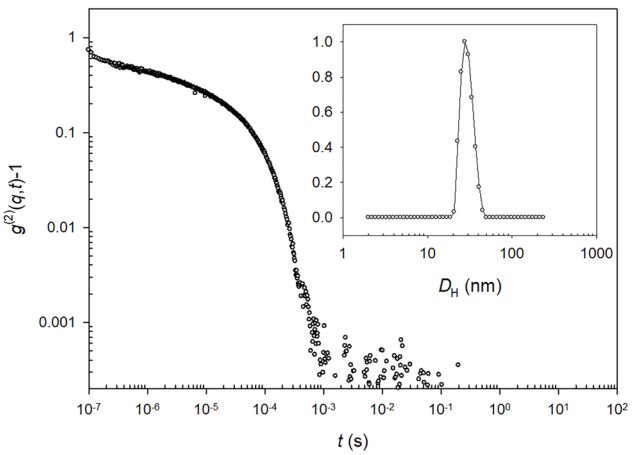

Fig. 2 Normalized intensity autocorrelation function obtained by light scattering at scattering angle θ = 90° for a 1 g l^{-1} HisBD solution at pH 5 in acetic acid buffer (100 mM). The inset represents the hydrodynamic diameter (D_H) distribution obtained by applying the Contin method to the data.

determination of the cooperative diffusion coefficient and of the D_H of the biodynamers (see Table 1). As the solutions are rather polydisperse with a polydispersity index ranging between 0.5 and 0.7, depending on the samples, the cumulant method, which is more sensitive to the short-time range of the correlation function (and thus to smaller species), gives lower values for D_H. The Contin method, sensitive to all species, is here a more appropriate method that allows determination of the average D_H with higher accuracy (see inset of Fig. 2). The determined values, M_w and D_H, strongly depend on the nature of the biodynamer. M_w ranges between 32 kDa for ArgBD and approximately 213 kDa for HisBD. Concomitantly, the evaluation of D_H revealed values ranging from approximately 11 nm to more than 30 nm, signifying that the biodynamers exhibit characteristics of low nanoscale systems. Intriguingly, as seen in our previous study, the incorporation of various amino acid side chains is known to induce diverse polymer sizes and elongation behaviors, giving rise to significant differences among the biodynamers.[8]

Table 1 Characterization of the biodynamers with a concentration of 1 mg mL^{-1} in pH 5 acetic acid buffer (100 mM) by dynamic lights scattering (DLS) and static light scattering (SLS). R_{excess}, excess Rayleigh ratio; M_w, weight-average molecular weight; DP, degree of polymerization; DH, hydrodynamic diameter obtained by applying the Contin method to our data. Error is 10%

Parameter	HisBD	LysBD	ArgBD	AspBD	GluBD
R_{excess} (cm^{-1})	25.63×10^{-6}	15.76×10^{-6}	3.94×10^{-6}	4.98×10^{-6}	7.60×10^{-6}
c (g cm^{-3})	10^{-3}	10^{-3}	10^{-3}	10^{-3}	10^{-3}
Polymer M_W (g mol^{-1})	213 583	131 333	32 833	41 500	63 333
Repeating unit M_W (g mol^{-1})	634.31	625.35	653.35	611.27	626.30
DP	337	210	50	68	101
D_H (nm)	30.5	25	13.8[a]	11	14.52

[a] For the ArgBD statistics is poorer due to a lower scattering level giving a larger error bar.

As mentioned in the introduction, the stabilizing effect of the CA core and HG shell on the carbazole moiety enables biodynamers to maintain stability in neutral and basic environment despite their dynamic nature. This stability is evidenced by consistent *Z*-Average and PDI values. To confirm these previous results, a one month long stability study for HisBD in a phosphate buffer (pH 7.4) using DLS analysis was conducted.

As shown in Fig. S2,† no significant change in *Z*-Average was observed during the first 14 days of measurement. However, at 21 days, the *Z*-Average consistently and significantly increased ($p < 0.05$). Throughout the measurement, the PDI remained relatively stable, indicating no significant change. The increase of *Z*-Average, however, strongly suggests an increase of instability under the experimental conditions after 14 days of measurement. In conclusion, this study confirms previous results that HisBD remains stable in a pH 7.4 environment for at least 14 days.[20]

Metal ion-selectivity and -sensitivity of biodynamers

By analyzing the fluorescence changes of diverse amino acid-based biodynamers with essential physiological cations (0.5 equiv. of Na(I), K(I), Mg(II), Ca(II), Co(II), Fe(II), Fe(III), Zn(II), and Cu(II)), we aimed to investigate two major aspects: first, the ions' affinity towards imines and acylhydrazones, present in the backbone of all biodynamers.[24,25,48] Second, an additional ion-selective effect towards the polymers' side chains (see Scheme 1) evidenced by either a fluorescence enhancing or quenching effect.[61] To each of the five biodynamers, 0.5 equivalents of each of the metal ions were added in 10 mM phosphate buffer (pH 7.4). Evaluating the experiment, the relative fluorescence depletion (%) without and upon ion-introduction was compared. As shown in Fig. 3, Na(I), K(I), Mg(II), Ca(II), and Co(II) do not exhibit any effect on the polymers' fluorescence. While Fe(II), Fe(III) and Zn(II) partly lead to a slight change in fluorescence, HisBD maintains at least 84% fluorescence upon the introduction of each respective ion. The slight decrease in HisBD fluorescence can be explained by weak ion interactions with the carbazole, imine and the imidazole side chains.[62–64] Evaluating the results, the Cu(II)-induced quenching effect was most evident for all biodynamers. This result suggests that the imines and acylhydrazones present in all biodynamers act as preferred binding sites affecting fluorescence, consistent with previously mentioned

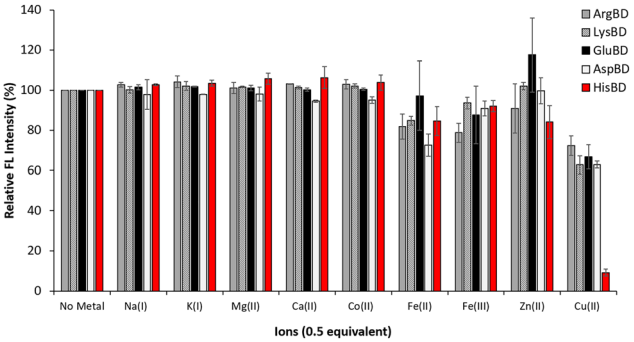

Fig. 3 Relative fluorescence depletion in percent (with I_0 = 100%) after introducing 0.5 equivalents of metal ions (50 μM) to each biodynamer (100 μM). Data represented as mean ± SD: (n = 3).

studies and our predicted outcomes from the AutoDock MD *in silico* analysis (Fig. 1). Furthermore, our results highlight the significance of the dynamic backbone for Cu(II)-induced quenching. As seen in Fig. 3, the fluorescence quenching on all biodynamers is selective to Cu(II). For 100 μM HisBD, the resulting fluorescence depletion reached approximately 90% upon the addition of 50 μM of Cu(II). In Fig. 4(A), the results

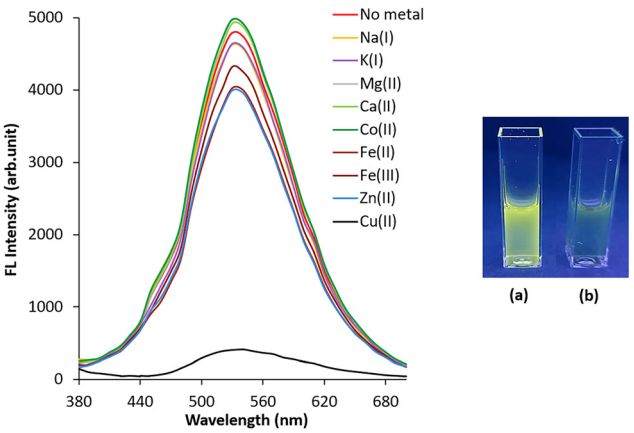

Fig. 4 (A) Addition of different metal ions (1 : 2 molar ratio) to HisBD with 50 μM Cu(II) showing a strong quenching effect on the fluorescence. Picture (B): Visualization of (a) HisBD (100 μM) in pH-neutral aqueous solution (pH 7.4) and (b) Cu(II) (50 μM or 1 : 2 equivalents) induced quenching effect at an λ_{ex} of 366 nm *via* a UV-lamp.

from Fig. 3 are supported, showing the emission spectrum of HisBD in the presence of different metal ions at λ_{ex} = 310 nm and λ_{em} = 525 nm and underlining the Cu(II) selective quenching. Additionally, as shown in Fig. 4(B), the respective quenching effect can be visualized by applying a UV lamp to the respective samples (λ_{ex} = 365 nm). In comparison, the addition of Cu(II), even at higher concentrations, did not cause any observable change in fluorescence on the fluorescent monomer CA-HG (see Fig. S6†). In conclusion, we observed a Cu(II)-selective interaction characterized by fluorescence quenching across all evaluated types of biodynamers. This underlines the ion-selectivity towards the imine and acylhydrazone groups present in all biodynamers, demonstrating comparability to previous studies regarding on–off Cu(II)-selective chemosensors.[17,49,65,66] Furthermore, supported by Hecel *et al.*, our results indicate that the interaction between the biodynamer and Cu(II) is not solely dependent on the presence of DCC groups on the polymer's backbone, but that the histidine side chain plays a critical role for the ion-to-polymer interaction as well.[67]

In silico simulation of Cu(II) affinity towards HisBD

For the AutoDock Vina MD prediction model, we considered only two His-hydrazides linked to a single CA-HG to enable rapid and efficient calculations. However, this approach made it challenging to observe the effects of repeating units within the polymer. Therefore, we investigated the binding affinity towards Cu(II) ions, with particular attention to the side chains of HisBD, using *in silico* models generated by the Molecular Operating Environment (MOE) software. MOE is frequently used for visualization of receptor active sites and calculation of receptor–ligand interactions, improving knowledge for potential ligand candidates.[68] It can, however, also be operated to simulate metal ions to ligand affinity.[69] Here, the probability of interactions of one Cu(II) to five repeating units of HisBD (excluding HG to reduce calculation volume) was assessed by calculating different polymer conformations (conformers) and the affiliated potential energy as well as the ion-polymer bond length.

After performing the simulation and displaying the most favorable conformation by choosing the lowest energy conformers of the ligand (HisBD) together with the central ion (Cu(II)), as previously confirmed by the AutoDock simulation (Fig. 1), the results showed an interaction of acylhydrazone and imine bonds by showing the bond length of 2.38–2.75 Å. This shows again the favored interaction of the ion with the fluorophore resonance system causing depletion of the fluorescence as observed in Fig. 4. Additionally, shown on the alignment of the five repeating units of HisBD (Fig. 5), displaying the most favorable energy state, the imidazole rings of the histidine-side chain show clear affinity towards Cu(II). By evaluating the number of functional groups per repeating unit that displayed a likelihood of interacting with one Cu(II), we consider the molar ratio of ion-to-polymer interaction to be approximately 1 : 2.5 (ion to repeating unit of HisBD).

When comparing the MOE simulation results with previous reliable X-ray-based methods, it was determined that one Cu

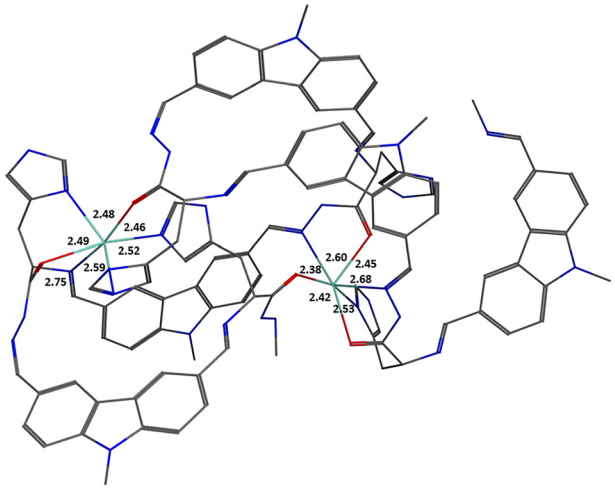

Fig. 5 *In silico* simulation *via* the software molecular operating environment (MOE): five repeating units of HisBD with two Cu(II) (green) with the affiliated distances in Angstrom (Å) of the metal ion to functional groups (heteroatoms) of the biodynamer. The simulation shows the conformation of the partial polymer and interaction sites of hydrogen (red) and nitrogen (blue) moieties with Cu(II).

(II)–O bond exhibited 30% covalent character, with a bond length ranging from 1.95 to 2.56 Å.[70] Supported by Burgos-Lopez *et al.*, this evaluation underlines that O-rich functional groups, including acylhydrazones, are strong coordinators of Cu(II).[71] Regarding the importance of the imidazole on the side chain, histidine is well known as a binding site to Cu(II).[72,73] Here, the ions' d-orbitals and the LUMO orbitals on the Schiff Base (here imidazole) contribute to the bonding.[74,75] Furthermore, the interaction between the orbitals can lead to a Cu(II)-induced quenching effect.[75]

In conclusion, the MOE *in silico* data is consistent with our AutoDock MD simulation and cuvette experiments, highlighting the importance of dynamic functional groups, specifically imines and acylhydrazones, for Cu(II) chelation. These findings align with previous reports by Berhanu *et al.* and Shi *et al.* on Schiff base-type Cu(II) sensors, where imine and acylhydrazone groups were also identified as key binding sites for Cu(II).[46,48] Additionally, the results emphasize that, due to the stabilizing effect of its imidazole group, HisBD exhibits the strongest binding affinity toward Cu(II). While Cu(II)-imidazole coordination is well-documented in biological systems, particularly with histidine, the simultaneous coordination of imine, acylhydrazone, and imidazole groups with Cu(II) is rarely reported.[76] Our evaluation suggests that this unique combination of functional groups, along with the polymer's conformation, leads to enhanced stability for the HisBD-Cu(II) complex compared to other Cu(II)-affine polymers.

Influence and importance of HG-chains for Cu(II)-binding

As discussed, due to the presence of CA, HisBD consists of a hydrophobic core.[8] Considering the hydrophobicity of the binding site, we questioned the accessibility of the ions to the hydrophobic core. Therefore, we further investigated the

importance of other functional groups, such as HG, for ion binding interactions. As seen in Fig. 5, HG was removed from the calculation, due to its freely rotating bonds which led to an extreme increase in calculation time. However, HG should not be neglected as it surrounds the biodynamers, leading to the hydrophilic shell.[8] Thus, when Cu(II) reaches the polymer to bind to near CA on its core side, it first encounters the HG-shell. We, therefore, speculate that the hydrophilic shell of the HisBD also plays a role in the initial binding of biodynamers to Cu(II).

As reported by Stoychev *et al.*, the electron-rich oxygen atoms in the backbone structure provide favorable coordination sites, enabling polyethylene glycols to effectively bind metal cations such as Cu(II) through interactions with oxygen's electron shells, potentially involving an ion-dipole mechanism.[77] Given the evaluation of the oxygen affinity in ether functional groups towards Cu(II) using the AutoDock Vina MD simulation (see Fig. S7†), we propose that the presence of HG around the polymer may induce an "ion-recruitment" effect. This effect potentially brings Cu(II) closer to the hydrophobic core, facilitating additional ion interactions due to the reduced distance to the chelating functional groups on the backbone and the imidazole-rich side chains of HisBD. As a result, HisBD shows increased sensitivity and selectivity towards Cu (II). This hypothesis, however, requires experimental validation, for example, using HG-deficient biodynamers. Yet, the absence of HG significantly affects the water solubility of biodynamers, making it difficult to compare the influence of HG on ion binding under aqueous conditions.

Ion-competing study

To further investigate the Cu(II) selectivity towards HisBD, we assessed the competitive binding behavior of different metal ions in 10 mM phosphate buffer (pH 7.4). In the specific case of on–off chemosensors, the ion-selectivity is evidenced by a selective fluorescence quenching effect despite the presence of other ions.[44,52,66] Therefore, we monitored the Cu(II)-induced quenching in the presence of physiological important metal-ions, Na(I), K(I), Mg(II), Co(II), Ca(II), Fe(II), Fe(III) and Zn(II). We analyzed the change in fluorescence first upon the introduction of the respective competing ions and then after adding Cu (II) at an equivalent of 0.5 molar of HisBD. The experiment was conducted in 10 mM pH 7.4 phosphate buffer. All samples were measured at λ_{ex} = 310 nm and λ_{em} = 525 nm. As demonstrated in Fig. 3 and 6, the addition of 50 μM of the respective metal ions (0.5 equiv. to HisBD) resulted in no more than a 16% fluorescence quenching effect (Fe(II)) on our HisBD. Upon the introduction of Cu(II) to each of the respective samples, however, an immediate decrease in fluorescence intensity of ~90% on HisBD was observed. The results did not only confirm the sensitivity of HisBD to Cu(II) ions but also emphasize its selectivity for Cu(II) even in the presence of other metal ions within the same sample, making our system comparable in selectivity towards recently reported on–off Cu (II) sensors.[17,49,65]

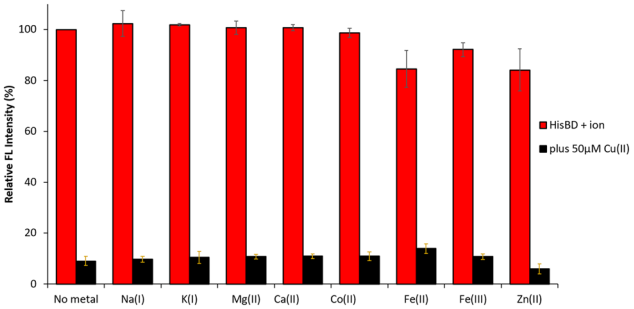

Fig. 6 Competing study of physiologically important metal ions on HisBD. Diagram of fluorescence depletion after an addition of different metal ions and an addition of Cu(II) (1 : 2 molar ratio) to the same sample afterwards (relative fluorescence, %). The red bars represent the fluorescence intensity of HisBD in the presence of various metal ions. The black bars represent the intensity of HisBD upon further addition of 0.5 equivalent Cu(II) to the same samples. Data represent as mean ± SD: (n = 3).

Cu(II)-induced quenching mechanisms

As reviewed by Sharma *et al.*, paramagnetic metals typically cause quenching through photoinduced electron transfer (PET) from an excited singlet state fluorophore to the paramagnetic metal centers.[78] During the PET process, the fluorophore (acceptor) and ligand (donor) are critical. These components, whether within the same structure or connected by a linker, undergo photoexcitation, causing an electron to transition from HOMO to LUMO in the fluorophore and creating a HOMO hole. This hole is filled by an electron from the ligand *via* an internal redox reaction, preventing the LUMO electron from returning to its ground state and significantly reducing the fluorophore's emission. In chemosensors, strong fluorescence is observed when electron transfer from the ligand to the fluorophore is absent.[78] However, PET can be induced by metal ion binding, resulting in chelation-enhanced quenching (CHEQ) or a "turn-off" response.[52] Bhattacharya *et al.* reported an imidazole-based Cu(II)-selective "turn-off" chemosensor, highlighting the significance of the histidine function.[79] Therefore, we suggest that HisBD can be classified as an on–off sensor, potentially susceptible to quenching *via* PET. Nonetheless, additional studies are required to fully validate this claim.

Fluorescence recovery upon the addition of a competing Cu(II) chelator

In addition to high ion-selectivity and sensitivity, reversibility is a valuable characteristic of Cu(II) sensors. Certain metal ions can oxidize unstable molecules with oxidizable functional groups, causing fluorescence quenching due to molecular destruction rather than ion coordination-based mechanisms. Therefore, the ability of the sensor to revert from the quenched state to its original fluorescence is essential. This ensures that the binding interaction does not irreversibly alter the sensor, thereby maintaining its reusability. As mentioned by Wang *et al.*, strong, competing Cu(II) chelators can be used to deter-

mine the sensor's reversibility, which is demonstrated by the restoration of fluorescence of the chelator.[80] Disodium ethylenediaminetetraacetate (EDTA-Na_2) has been proven to show a strong affinity towards a variety of transition metal ions, including Cu(II).[81] Showing a stability constant of $K = 2.5 \times 10^3$ L mol^{-1}, the bidental chelator forms Cu(II)-complexes at a molar ratio of 1 : 1 in neutral, aqueous solution, indicating a high level of complex stability.[82,83] Thus, we investigated the fluorescence changes of Cu(II)-binding to HisBD upon the addition of EDTA-Na_2 as a competing chelator in order to investigate the reversibility of the Cu(II)-induced fluorescence quenching effect on HisBD. Starting the experiment, EDTA-Na_2 was titrated to a previously prepared HisBD and Cu(II) mixture of 1 : 2 molar ratio (ion : biodynamer) with concentrations ranging from 3.13 μM (1 : 20 equivalents) up to 100 μM (1 : 1 equivalent) (Fig. 7(A)). Adding 3.13 μM EDTA-Na_2 solution, a fluorescence recovery of around 5% was measured (from a quenched fluorescence of 14.2%, back up to 19.2% fluorescence). However, after doubling the concentration of EDTA-Na_2 up to 6.25 μM, a jump in fluorescence recovery up to 44.7% of the initial fluorescence was observed. Increasing the concentration further up to 100 μM EDTA-Na_2, a stagnation in fluorescence recovery was noticed. The introduction of 100 μM EDTA-Na_2 led to a final fluorescence recovery of around 70% (Fig. 7(B)(a)–(h)). Discussing the results, the addition of a 1 : 1 molar ratio of EDTA-Na_2 resulted in a rapid, clearly visual fluorescence recovery of HisBD.

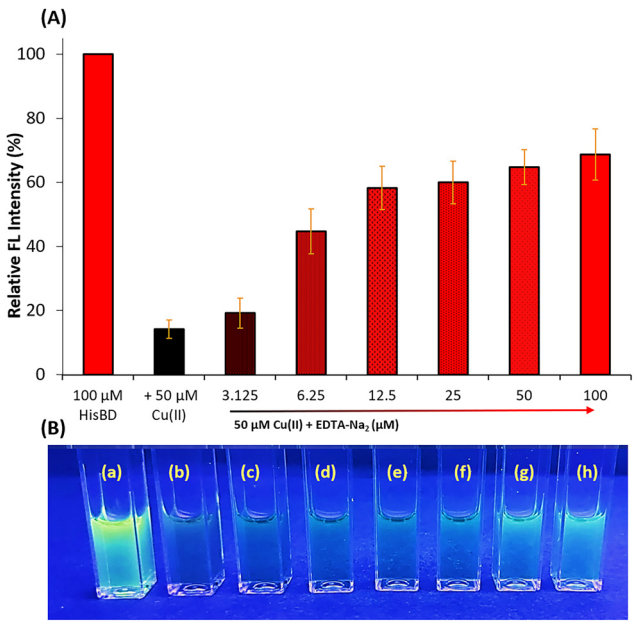

Fig. 7 (A) Fluorescence recovery of quenched HisBD (100 μM, with 50 μM of Cu(II)) caused by the addition of competing chelator, ethylenediaminetetraacetic acid (EDTA-Na_2). Data represent as mean ± SD: (n = 3). (B) Visualization of ETDA-induced fluorescence recovery of each sample represented in (A) using a UV-Vis lamp with an excitation of 366 nm, (a) 100 μM HisBD (b) 100 μM HisBD + 50 μM Cu(II), and (c)–(h) 100 μM HisBD + 50 μM Cu(II) with increasing amount of EDTA-Na_2.

Achieving a complete fluorescence recovery to 100% remained unattainable, likely due to the partial fluorescence-quenching effect of EDTA-Na_2 on HisBD, as illustrated in Fig. S8.† In conclusion, the fluorescence of HisBD can be chemically restored by introducing a strong competing Cu(II) chelator. This result aligns with previously reported on–off Cu(II) sensors.[80,84] Furthermore, this observation provides preliminary evidence of the polymer's notable complex stability with Cu(II) ions.

To highlight the polymer's integrity upon Cu(II) chelation regarding its reusability, we additionally compared the molecular weight (M_w) of HisBD (10 mM) in 10 mM phosphate buffer (pH 7.4) before and after the addition of Cu(II) at a 1 : 2 molar ratio using static light scattering (SLS) analysis (see Fig. S3†). Comparing the samples, no significant change in M_w of HisBD was observed upon Cu(II) introduction. Since changes in M_w, particularly for dynamic polymers, indicate instability or degradation, this result confirms the stability of HisBD upon the addition of Cu(II) in an aqueous pH 7.4 environment.[85]

Cu(II) concentration-dependent fluorescence depletion

After we confirmed the selective Cu(II)-induced fluorescence quenching effect on HisBD, we evaluated the concentration-dependent depletion of the fluorescence, aiming to determine the detection limits of our system under physiological conditions (Fig. 8(A)).

For this experiment, the quotient of the initial fluorescence (I_0) with the fluorescence after adding Cu(II) was plotted against the concentration of Cu(II) in μM. Here, Cu(II) concentrations, spanning from 1.56 μM to 100 μM, were each added to a solution of 100 μM HisBD and analyzed at λ_{ex} = 310 nm and λ_{em} = 525 nm in a 96-well plate using a Tecan reader. To highlight the potential biological application of our system, we conducted this experiment in OptiMEM cell medium (pH 7.4). Given that the decrease in fluorescence dependent on Cu(II) plateaued beyond a 1 : 1 molar ratio, we assessed a linear fluorescence depletion with metal ion concentration up to 100 μM Cu(II). The lowest evaluated concentration was set to 1.56 μM, which lies within the range of the targeted application.

As seen in Fig. 8(B), the fluorescence was quenched proportional to the added amounts of Cu(II) until 1 : 1 equivalent was added (100 μM), resulting in a R^2-value of 0.975. Our quantification method enables reliable detection of low Cu(II) concentrations down to 1.56 μM, demonstrating the high sensitivity of HisBD towards Cu(II) under physiological conditions. Previous studies on organic Cu(II) sensors have reported Cu(II) detection limits ranging from 7.3×10^{-4} to 100 μM.[46] Therefore, the threshold of 1.56 μM, evaluated in our study at pH 7.4 in OptiMEM medium, falls within this range, demonstrating its comparability to previous sensors with high ion-sensitivity.[46] In conclusion, this experiment demonstrated that Cu(II) quantification *via* HisBD in cell medium at concentrations as low as 1.56 μM is achievable, providing a promising outlook for future applications. However, free Cu(II) ions in blood serum are typically present at concentrations below the

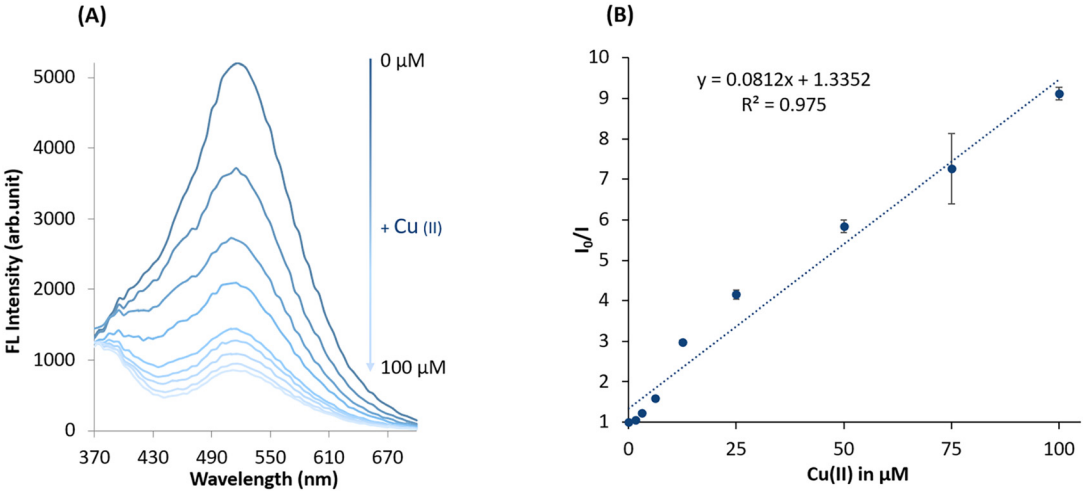

Fig. 8 Concentration-dependent fluorescence quenching *via* Cu(II) on HisBD. (A) Decrease of fluorescence *via* an increase of added Cu(II) on HisBD (100 μM). (B) Fluorescence intensity changes of HisBD (in I_0/I) by Cu(II) concentration. I_0 represents the starting fluorescence intensity of HisBD (100 μM), and I the fluorescence intensity after the addition of Cu(II). Data represented as mean ± SD: (n = 3).

detection threshold of HisBD, as they are usually bound to proteins like human serum albumin.[86] Therefore, further research is necessary to validate the sensitivity of HisBD as Cu(II) sensors in biological systems, particularly for detecting Cu(II) as a disease biomarker.

Biocompatibility

In our previous publications, the biocompatibility of different biodynamers such as LysBD, HisBD, and ArgBD was confirmed by performing MTT assays in buffer (HBSS) and *in vivo* toxicity studies in zebrafish larvae.[11] To strengthen earlier results and underline the Cu(II)-sensors biocompatibility, a MTT assay-based cell viability experiment was conducted. This assay involved a 24-hour and a 48-hour-treatment period using A549 epithelial carcinoma cells.

As described in Fig. 9, the cells underwent treatment with various concentrations of HisBD, LysBD, and ArgBD up to 500 μg mL^{-1}. For LysBD and ArgBD, the results of the 24-hour assay indicate that cell viability remains relatively stable at the tested concentrations. Even at the highest concentration of 500 μg mL^{-1}, there was no noticeable decline in cellular viability following treatment with the respective polymers. In the case of HisBD, the polymer exhibits a slight increase in cytotoxicity compared to LysBD and ArgBD, which may be due to its high M_w (6.6-fold higher M_w than that of ArgBD). It is well known that the toxicity of polymers increases with increasing

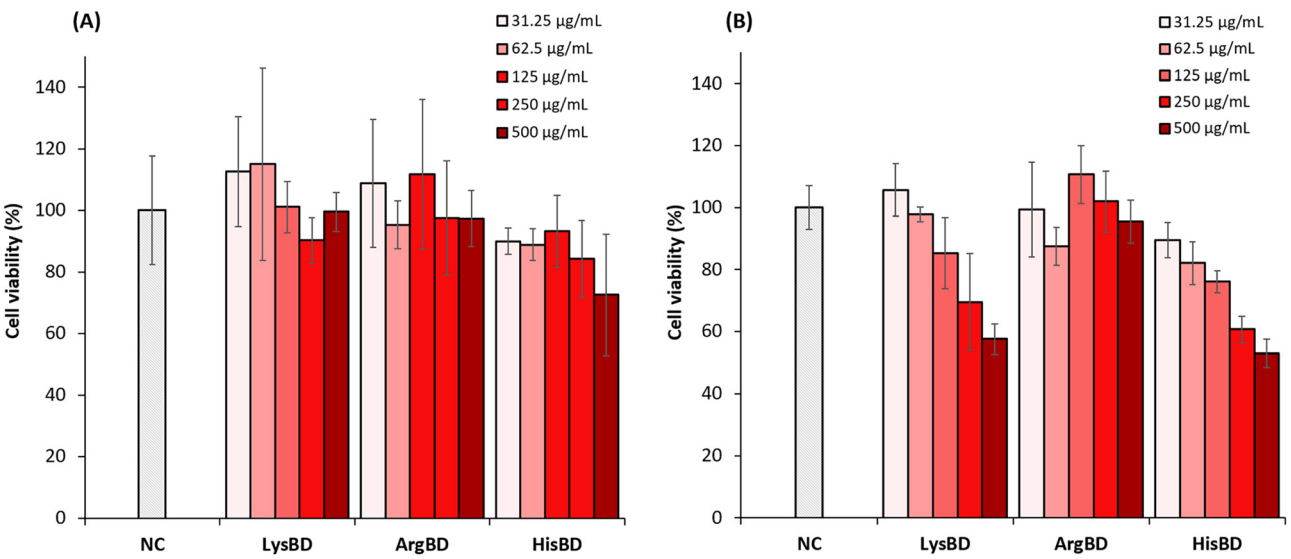

Fig. 9 Cell viability study comparing the negative control (NC) with HisBD, LysBD, and ArgBD. The MTT assay was conducted using an A549 cell line. Each sample was treated for (A) 24 hours and (B) 48 h at the specified concentration. Data represented as mean ± SD: (n = 3).

M_w.[11,87] Hence, the biocompatibility of the examined biodynamers was confirmed at the tested concentration (100 μM) for Cu(II) binding, and by controlling the M_w of the biodynamers, it is anticipated that their toxicity can be further reduced. Evaluating the results of the 48-hour assay, the cytotoxicity for HisBD and LysBD increased compared to the 24-hour assay (see Fig. 9(B)), while the cytotoxicity of ArgBD remained relatively stable. At the highest concentration of 500 μg mL^{-1}, cell viability was 57.6% for LysBD and 52.9% for HisBD. The concentration at which HisBD is applied as a Cu(II) sensor is 100 μM, equivalent to 63.5 μg mL^{-1} (see Fig. 8 and Table 1). At this concentration, after 48 hours of treatment, cell viability remains above 82%. Despite the observed decline in cell viability over time, the results indicate that HisBD maintains sufficiently biocompatible, particularly as a rapid Cu(II) sensor at the specified concentration. According to Lee *et al.*, the increase in cell toxicity observed over 48 hours can be attributed to the release of free monomer CA-HG resulting from time-dependent degradation.[11] Additionally, it is important to recognize that the ion chelating properties of Cu(II) sensors could influence the viability of the cells.[88,89] However, further investigation is necessary to determine whether this mechanism contributes to a change in toxicity regarding our system.

Conclusions

In this study, we confirmed the affinity of HisBD towards Cu(II), evidenced by the notable selective fluorescence Cu(II)-induced quenching. *In silico* modeling and spectroscopic analysis of the biodynamer's Cu(II)-dependent fluorescence, irrespective of the amino acid side chain type, identified acylhydrazones and imines as key binding sites for Cu(II). These groups are linked to the fluorophore and are a crucial part of DCC. Additionally, we confirmed that the presence of imidazoles in the side chain of HisBD enhances its sensitivity towards Cu(II) compared to other biodynamers. We discussed how the nanostructure and HG shell enhance ion-sensitivity and developed a Cu(II) quantification method in cell medium with a threshold of 1.56 μM. Overall, HisBD was demonstrated as an effective polymer-based Cu(II)-sensing agent with reversible character, exhibiting excellent biocompatibility, solubility, and ion sensitivity in aqueous solutions – properties that are rarely achieved simultaneously in a single system. In conclusion, this study presents the first report of a fluorescent, histidine-derived, biodynamer-based Cu(II) ion sensor, thus expanding the field of DCC and biodynamer research into nano-sized, ion-recognition systems.

Author contributions

Sangeun Lee conceived the idea, designed the experiments, and supervised the project. Lena Zeroug-Metz and Sangeun Lee wrote, edited, and revised the manuscript together with Eric Buhler, Bo Hyun Ryu and Mohamed A. Kamal. Lena Zeroug-Metz conducted the majority of the experiments. Eric Buhler conducted the SLS and DLS measurements. Bo Hyun Ryu and Kalanika Elamaldeniya conducted the AutoDock MD *in silico* experiments, Mohamed A. Kamal performed the MOE *in silico* simulations. Justine Bassil and Lena Zeroug-Metz synthesized the materials. All authors have given approval to the final version of the manuscript.

Data availability

The data supporting this article have been included as part of the ESI.†

Conflicts of interest

The authors have no conflicts to declare.

Acknowledgements

Authors acknowledge M. Schneider from the Department of Pharmacy, B. Morgenstein and G. Kickelbick from the Department of Chemistry at Saarland University, for their support in instrument availability and engaging in discussions related to the structural analysis of ion-molecule binding.

References

1 E. Kolomiets and J.-M. Lehn, Double dynamers: molecular and supramolecular double dynamic polymers, *Chem. Commun.*, 2005, 1519–1521.
2 O. Ramström and J.-M. Lehn, In Situ Generation and Screening of a Dynamic Combinatorial Carbohydrate Library against Concanavalin A, *ChemBioChem*, 2000, 41–48.
3 A. Rodrigues, L. Rocard and R. Moumné, Peptide and Peptidomimetic Assemblies in Dynamic Combinatorial Chemistry, *ChemSystemsChem*, 2023, **5**, 1–18.
4 Y. Zhang, Y. Qi, S. Ulrich, M. Barboiu and O. Ramström, Dynamic Covalent Polymers for Biomedical Applications, *Mater. Chem. Front.*, 2020, **4**, 489–506.
5 O. Ramström, S. Lohmann, T. Bunyapaiboonsri and J.-M. Lehn, Dynamic combinatorial carbohydrate libraries: probing the binding site of the concanavalin A lectin, *Chem. – Eur. J.*, 2004, **10**, 1711–1715.
6 S. J. Rowan, S. J. Cantrill, G. R. L. Cousins, J. K. M. Sanders and J. Fraser Stoddart, Dynamic Covalent Chemistry, *Angew. Chem., Int. Ed.*, 2002, **2002**, 898–952.
7 J.-M. Lehn, Dynamic Combinatorial Chemistry and Virtual Combinatorial LibrariesAdapted from: J.-M. Lehn, Chem. Eur.19995, *Chem. – Eur. J.*, 1999, **5**, 2455.
8 Y. Liu, M. C. A. Stuart, E. Buhler, J.-M. Lehn and A. K. H. Hirsch, Proteoid Dynamers with Tunable Properties, *Adv. Funct. Mater.*, 2016, **26**, 6297–6305.

9 Y. Liu, M. C. A. Stuart, E. Buhler and A. K. H. Hirsch, Dynamic Proteoids Generated From Dipeptide-Based Monomers, *Macromol. Rapid Commun.*, 2018, **39**, 1800099.
10 H. Ying, Y. Zhang and J. Cheng, Dynamic urea bond for the design of reversible and self-healing polymers, *Nat. Commun.*, 2014, **5**, 3218.
11 S. Lee, S. Nasr, S. Rasheed, Y. Liu, O. Hartwig, C. Kaya, A. Boese, M. Koch, J. Herrmann, R. Müller, B. Loretz, E. Buhler, A. K. H. Hirsch and C.-M. Lehr, Proteoid biodynamers for safe mRNA transfection via pH-responsive nanorods enabling endosomal escape, *J. Controlled Release*, 2023, **353**, 915–929.
12 Y. Liu, S. Ashmawy, L. Latta, A.-V. Weiss, A. F. Kiefer, S. Nasr, B. Loretz, A. K. H. Hirsch, S. Lee and C.-M. Lehr, pH-Responsive Dynaplexes as Potent Apoptosis Inductors by Intracellular Delivery of Survivin siRNA, *Biomacromolecules*, 2023, **24**, 3742–3754.
13 Y. Liu, T. Hamm, T. R. Eichinger, W. Kamm, H. A. Wieland, B. Loretz, A. K. H. Hirsch, S. Lee and C.-M. Lehr, Biodynamer Nano-Complexes and -Emulsions for Peptide and Protein Drug Delivery, *Int. J. Nanomed.*, 2024, **19**, 4429–4449.
14 M. A. M. Kamal, J. Bassil, B. Loretz, A. K. H. Hirsch, S. Lee and C.-M. Lehr, Arg-biodynamers as antibiotic potentiators through interacting with Gram-negative outer membrane lipopolysaccharides, *Eur. J. Pharm. Biopharm.*, 2024, **200**, 114336.
15 O. Ramström and J.-M. Lehn, Drug discovery by dynamic combinatorial libraries, *Nat. Rev. Drug Discovery*, 2002, **1**, 26–36.
16 Y. Zhang and M. Barboiu, Ligand Mediated Metal Cations Exchanges within Metallo-Dynameric Solid Films, *ChemistryOpen*, 2019, **8**, 1345–1349.
17 M. Aarjane, S. Slassi and A. Amine, Novel highly selective and sensitive fluorescent sensor for copper detection based on N-acylhydrazone acridone derivative, *J. Mol. Struct.*, 2020, **1199**, 126990.
18 Y. Liu, J.-M. Lehn and A. K. H. Hirsch, Molecular Biodynamers: Dynamic Covalent Analogues of Biopolymers, *Acc. Chem. Res.*, 2017, **50**, 376–386.
19 T. Peker, B. Zagiel, L. Rocard, C. Bich, E. Sachon and R. Moumné, Analytical Tools for Dynamic Combinatorial Libraries of Cyclic Peptides, *ChemBioChem*, 2023, **24**, e202300688.
20 A. K. H. Hirsch, E. Buhler and J.-M. Lehn, Biodynamers: Self-Organization-Driven Formation of Doubly Dynamic Proteoids, *J. Am. Chem. Soc.*, 2012, **134**, 4177–4183.
21 S. Lee, C. Kaya, H. Jang, M. Koch, B. Loretz, E. Buhler, C.-M. Lehr and A. K. H. Hirsch, pH-Dependent morphology and optical properties of lysine-derived molecular biodynamers, *Mater. Chem. Front.*, 2020, **4**, 905–909.
22 I. Hwang, I. Hong, K.-S. Jeong and W.-D. Jang, Carbazole-based molecular tweezers as platforms for the discrimination of heavy metal ions, *RSC Adv.*, 2015, **5**, 1097–1102.
23 H.-C. Gee, C.-H. Lee, Y.-H. Jeong and W.-D. Jang, Highly sensitive and selective cyanide detection via Cu2+ complex ligand exchange, *Chem. Commun.*, 2011, **47**, 11963–11965.
24 F. Kolcu and İ. Kaya, Carbazole-based Schiff base: A sensitive fluorescent 'turn-on' chemosensor for recognition of Al (III) ions in aqueous-alcohol media, *Arabian J. Chem.*, 2022, **15**, 103935.
25 A. Feng, P. Liu, Q. Liang, X. Zhang, L. Huang, Y. Jia, M. Xie, Q. Yan, C. Li and S. Wang, A new carbazole-based colormetric and ratiometric fluorescent probe for hypochlorite sensing in living cells and zebrafishes, *Dyes Pigm.*, 2020, **180**, 108492.
26 L. Hong, T. M. Carducci, W. D. Bush, C. G. Dudzik, G. L. Millhauser and J. D. Simon, Quantification of the binding properties of Cu2+ to the amyloid beta peptide: coordination spheres for human and rat peptides and implication on Cu2+-induced aggregation, *J. Phys. Chem. B*, 2010, **114**, 11261–11271.
27 É. Józsa, K. Ősz, C. Kállay, P. de Bona, C. A. Damante, G. Pappalardo, E. Rizzarelli and I. Sóvágó, Nickel(II) and mixed metal complexes of amyloid-ß-N-terminus, *Dalton Trans.*, 2010, **39**, 7046–7053.
28 D.-H. Cai, B.-H. Chen, Q.-Y. Liu, X.-Y. Le and L. He, Synthesis, structural studies, interaction with DNA/HSA and antitumor evaluation of new Cu(II) complexes containing 2-(1H-imidazol-2-yl)pyridine and amino acids, *Dalton Trans.*, 2022, **51**, 16574–16586.
29 A. M. Abu-Dief, L. H. Abdel-Rahman, A. A. Abdelhamid, A. A. Marzouk, M. R. Shehata, M. A. Bakheet, O. A. Almaghrabi and A. Nafady, Synthesis and characterization of new Cr(III), Fe(III) and Cu(II) complexes incorporating multi-substituted aryl imidazole ligand: Structural, DFT, DNA binding, and biological implications, *Spectrochim. Acta, Part A*, 2020, **228**, 117700.
30 B.-E. Kim, T. Nevitt and D. J. Thiele, Mechanisms for copper acquisition, distribution and regulation, *Nat. Chem. Biol.*, 2008, **4**, 176–185.
31 J. Chen, Y. Jiang, H. Shi, Y. Peng, X. Fan and C. Li, The molecular mechanisms of copper metabolism and its roles in human diseases, *Pflügers Arch.*, 2020, **472**, 1415–1429.
32 R. A. Festa and D. J. Thiele, Copper: An essential metal in biology, *Curr. Biol.*, 2011, **21**, R877–R883.
33 F. Focarelli, A. Giachino and K. J. Waldron, Copper microenvironments in the human body define patterns of copper adaptation in pathogenic bacteria, *PLoS Pathog.*, 2022, **18**, e1010617.
34 A. Gupte and R. J. Mumper, Elevated copper and oxidative stress in cancer cells as a target for cancer treatment, *Cancer Treat. Rev.*, 2009, **35**, 32–46.
35 K. Jomova, M. Makova, S. Y. Alomar, S. H. Alwasel, E. Nepovimova, K. Kuca, C. J. Rhodes and M. Valko, Essential metals in health and disease, *Chem.-Biol. Interact.*, 2022, **367**, 110173.
36 C. Mulligan and J. M. Bronstein, Wilson Disease: An Overview and Approach to Management, *Neurol. Clin.*, 2020, **38**, 417–432.
37 J. Nie, D. Feng, J. Shang, B. Nasen, T. Jiang, Y. Liu and S. Hou, Green composite aerogel based on citrus peel/chitosan/bentonite for sustainable removal Cu(II) from water matrices, *Sci. Rep.*, 2023, **13**, 15443.

38 Ç. Duygu, B. Nilay and D. Adil, Advanced Plasmonic Nanosensors for Monitoring of Environmental Pollutants, *Curr. Anal. Chem.*, 2023, **19**, 2–17.
39 R. Liu, P. Wu, L. Yang, X. Hou and Y. Lv, Inductively coupled plasma mass spectrometry-based immunoassay: a review, *Mass Spectrom. Rev.*, 2014, **33**, 373–393.
40 M. M. Rahman, K. A. Alamry, T. S. Saleh and A. M. Asiri, Sensitive and selective Cu2+ sensor based on 4-(3-(thiophen-2-yl)-9H-carbazol-9-yl)benzaldehyde (TPCBZ) conjugated copper-complex, *J. Organomet. Chem.*, 2016, **817**, 43–49.
41 G. Bagherian, M. Arab Chamjangali, H. Shariati Evari and M. Ashrafi, Determination of copper(II) by flame atomic absorption spectrometry after its perconcentration by a highly selective and environmentally friendly dispersive liquid–liquid microextraction technique, *J. Anal. Sci. Technol.*, 2019, **10**, 3.
42 D. Feng, T. Zhang, T. Zhong, C. Zhang, Y. Tian and G. Wang, Coumarin-embedded MOF UiO-66 as a selective and sensitive fluorescent sensor for the recognition and detection of Fe 3+ ions, *J. Mater. Chem. C*, 2021, **9**, 16978–16984.
43 T. Zhang, A. Salah, S. Chang, Z. Zhang and G. Wang, Study on the fluorescent covalent organic framework for selective "turn-off"recognition and detection of Fe3+ ions, *Tetrahedron*, 2021, **96**, 132405.
44 Y. He, J. Yin and G. Wang, New selective "on-off" fluorescence chemosensor based on carbazole Schiff base for Fe3+ detection, *Chem. Heterocycl. Compd.*, 2018, **54**, 146–152.
45 G. Sivaraman, M. Iniya, T. Anand, N. G. Kotla, O. Sunnapu, S. Singaravadivel, A. Gulyani and D. Chellappa, Chemically diverse small molecule fluorescent chemosensors for copper ion, *Coord. Chem. Rev.*, 2018, **357**, 50–104.
46 A. L. Berhanu, Gaurav, I. Mohiuddin, A. K. Malik, J. S. Aulakh, V. Kumar and K.-H. Kim, A review of the applications of Schiff bases as optical chemical sensors, *Trends Anal. Chem.*, 2019, **116**, 74–91.
47 Y. Jiao, X. Liu, L. Zhou, H. He, P. Zhou, C. Duan and X. Peng, A fluorescein derivative-based fluorescent sensor for selective recognition of copper(II) ions, *J. Photochem. Photobiol., A*, 2018, **355**, 67–71.
48 T. Shi, Z. Xie, X. Mo, Y. Feng, T. Peng, F. Wu, M. Yu, J. Zhao, L. Zhang and J. Guo, Synthesis and Application of Salicylhydrazone Probes with High Selectivity for Rapid Detection of Cu2, *Molecules*, 2024, **29**, 2032.
49 S. Gorai, A. Ghosh, S. Chakraborty, P. Retailleau, T. K. Ghanty, B. S. Patro and S. Mula, Fluorescent Cu2+ sensor based on phenanthroline-BODIPY conjugate: A mechanistic study, *Dyes Pigm.*, 2022, **203**, 110343.
50 S. Liu, Y.-M. Wang and J. Han, Fluorescent chemosensors for copper(II) ion: Structure, mechanism and application, *J. Photochem. Photobiol., C*, 2017, **32**, 78–103.
51 H. Lee, I. Hong and W.-D. Jang, Design and applications of molecular probes containing porphyrin derivatives, *Coord. Chem. Rev.*, 2018, **354**, 46–73.
52 A. Y. Alyami, Recent progress in organic fluorescence and colorimetric chemosensors for Cu2+ detection: A comprehensive review (2018–2023), *Dyes Pigm.*, 2023, **220**, 111740.
53 J. Wang, H. Li, H. Qin, Z. Su, G. Liu and S. Hou, A water-soluble benzimidazole derivative for rapidly detecting Cu2+ in aqueous solution, *J. Mol. Struct.*, 2023, **1274**, 134416.
54 H. Sun, Q. Xu, C. Xu, Y. Zhang, J. Ai, M. Ren, K. Liu and F. Kong, Construction of a water-soluble fluorescent probe for copper(II) ion detection in live cells and food products, *Food Chem.*, 2023, **418**, 135994.
55 N. Choudhury, B. Saha and P. De, Recent progress in polymer-based optical chemosensors for Cu2+ and Hg2+ Ions: A comprehensive review, *Eur. Polym. J.*, 2021, **145**, 110233.
56 J. Hu and S. Liu, Engineering Responsive Polymer Building Blocks with Host–Guest Molecular Recognition for Functional Applications, *Acc. Chem. Res.*, 2014, **47**, 2084–2095.
57 D. Santos-Martins, S. Forli, M. J. Ramos and A. Olson, AutoDock4Zn An improved AutoDock forcefield for small-molecule docking to zinc metalloproteins, *J. Chem. Inf. Model.*, 2014, **2014**, 1–34.
58 O. Trott and A. J. Olson, AutoDock Vina: Improving the Speed and Accuracy of Docking with a New Scoring Function, Efficient Optimization, and Multithreading, *J. Comput. Chem.*, 2010, **31**, 455–461.
59 J. Eberhardt, D. Santos-Martins, A. F. Tillack and S. Forli, AutoDock Vina 1.2.0: New Docking Methods, Expanded Force Field, and Python Bindings, *J. Chem. Inf. Model.*, 2021, **61**, 3891–3898.
60 N. Noorussabah, M. Choudhary, N. Das, B. Mohan, K. Singh, R. K. Singh, K. Ahmad, S. Muhammad and S. Kumar, Copper(II) and Nickel(II) Complexes of Tridentate Hydrazide and Schiff Base Ligands Containing Phenyl and Naphthalyl Groups: Synthesis, Structural, Molecular Docking and Density Functional Study, *J. Inorg. Organomet. Polym. Mater.*, 2020, **30**, 4426–4440.
61 P. Murugaperumal, P. Rajendran, S. Nallathambi, S. Ayyanar, F. Perdih, A. Balasubramaniem and A. Alagarsamy, An oxalamide-bridged imidazole based 'turn off' fluorescent receptor for copper(II) and iron(III) ions, *New J. Chem.*, 2023, **47**, 13342–13352.
62 S. Gülle and S. Çelik Erbaş, A Selective Fluorescence Sensor for Fe(III) Based on Phenanthroimidazole Imine Compound, *J. Fluoresc.*, 2018, **28**, 445–451.
63 X. Zhu, Y. Duan, P. Li, H. Fan, T. Han and X. Huang, A highly selective and instantaneously responsive Schiff base fluorescent sensor for the "turn-off" detection of iron(III), iron(II), and copper(II) ions, *Anal. Methods*, 2019, **11**, 642–647.
64 H. Kabeer, S. Hanif, A. Arsalan, S. Asmat, H. Younus and M. Shakir, Structural-Dependent N,O-Donor Imine-Appended Cu(II)/Zn(II) Complexes: Synthesis, Spectral, and in Vitro Pharmacological Assessment, *ACS Omega*, 2020, **5**, 1229–1245.
65 M.-Q. Wang, K. Li, J.-T. Hou, M.-Y. Wu, Z. Huang and X.-Q. Yu, BINOL-based fluorescent sensor for recognition of Cu(II) and Sulfide Anion in water, *J. Org. Chem.*, 2012, **77**, 8350–8354.

66 F. N. Arslan, G. A. Geyik, K. Koran, F. Ozen, D. Aydin, Ş. N. K. Elmas, A. O. Gorgulu and I. Yilmaz, Fluorescence "Turn On-Off" Sensing of Copper(II) Ions Utilizing Coumarin-Based Chemosensor: Experimental Study, Theoretical Calculation, Mineral and Drinking Water Analysis, *J. Fluoresc.*, 2020, **30**, 317–327.

67 A. Hecel, J. Wątły, M. Rowińska-Żyrek, J. Świątek-Kozłowska and H. Kozłowski, Histidine tracts in human transcription factors: insight into metal ion coordination ability, *J. Biol. Inorg. Chem.*, 2018, **23**, 81–90.

68 I.-J. Chen and N. Foloppe, Conformational Sampling of Druglike Molecules with MOE and Catalyst: Implications for Pharmacophore Modeling and Virtual Screening, *J. Chem. Inf. Model.*, 2008, **48**, 1773–1791.

69 N. F. Mahmoud, A. A. Abbas and G. G. Mohamed, Synthesis, characterization, antimicrobial, and MOE evaluation of nano 1,2,4−triazole–based Schiff base ligand with some d–block metal ions, *Appl. Organomet. Chem.*, 2021, **35**, 1–14.

70 G. Tamasi, L. Chiasserini, L. Savini, A. Sega and R. Cini, Structural study of ribonucleotide reductase inhibitor hydrazones. Synthesis and X-ray diffraction analysis of a copper(II)-benzoylpyridine-2-quinolinyl hydrazone complex, *J. Inorg. Biochem.*, 2005, **99**, 1347–1359.

71 Y. Burgos-Lopez, J. Del Plá, L. M. Balsa, I. E. León, G. A. Echeverría, O. E. Piro, J. García-Tojal, R. Pis-Diez, A. C. González-Baró and B. S. Parajón-Costa, Synthesis, crystal structure and cytotoxicity assays of a copper(II) nitrate complex with a tridentate ONO acylhydrazone ligand. Spectroscopic and theoretical studies of the complex and its ligand, *Inorg. Chim. Acta*, 2019, **487**, 31–40.

72 P. H. Walton, G. J. Davies, D. E. Diaz and J. P. Franco-Cairo, The histidine brace: nature's copper alternative to haem?, *FEBS Lett.*, 2023, **597**, 485–494.

73 S. Brander, I. Horvath, J. Ø. Ipsen, A. Peciulyte, L. Olsson, C. Hernández-Rollán, M. H. H. Nørholm, S. Mossin, L. Lo Leggio, C. Probst, D. J. Thiele and K. S. Johansen, Biochemical evidence of both copper chelation and oxygenase activity at the histidine brace, *Sci. Rep.*, 2020, **10**, 16369.

74 J.-M. Chen, W.-J. Ruan, L. Meng, F. Gao and Z.-A. Zhu, Spectroscopic and theoretical studies on axial coordination of bis(pyrrol-2-ylmethyleneamine)phenyl complexes, *Spectrochim. Acta, Part A*, 2008, **71**, 191–198.

75 A. Z. El-Sonbati, M. A. Diab, S. Morgan, M. I. Abou-Dobara and A. A. El-Ghettany, Synthesis, characterization, theoretical and molecular docking studies of mixed-ligand complexes of Cu(II), Ni(II), Co(II), Mn(II), Cr(III), UO2(II) and Cd(II), *J. Mol. Struct.*, 2020, **1200**, 127065.

76 F. Arrigoni, T. Prosdocimi, L. Mollica, L. de Gioia, G. Zampella and L. Bertini, Copper reduction and dioxygen activation in Cu-amyloid beta peptide complexes: insight from molecular modelling, *Metallomics*, 2018, **10**, 1618–1630.

77 D. Stoychev and C. Tsvetanov, Behaviour of poly(ethylene glycol) during electrodeposition of bright copper coatings in sulfuric acid electrolytes, *J. Appl. Electrochem.*, 1996, 741–749.

78 S. Sharma and K. S. Ghosh, Recent advances (2017-20) inthe detection of copper ion by using fluorescence sensors working through transfer of photo-induced electron (PET), excited-state intramolecular proton (ESIPT) and Förster resonance energy (FRET), *Spectrochim. Acta, Part A*, 2021, **254**, 119610.

79 A. Bhattacharya, S. Mahata, A. Bandyopadhyay, B. B. Mandal and V. Manivannan, Application of 2,4,5-tris (2-pyridyl)imidazole as 'turn-off' fluorescence sensor for Cu (II) and Hg(II) ions and in vitro cell imaging, *Luminescence*, 2022, **37**, 883–891.

80 H. Wang, B. Fang, Le Zhou, Di Li, L. Kong, K. Uvdal and Z. Hu, A reversible and highly selective two-photon fluorescent "on-off-on" probe for biological Cu2+ detection, *Org. Biomol. Chem.*, 2018, **16**, 2264–2268.

81 W. Maketon, C. Z. Zenner and K. L. Ogden, Removal Efficiency and Binding Mechanisms of Copper and Copper-EDTA Complexes using Polyethyleneimine, *Environ. Sci. Technol.*, 2008, **42**, 2124–2129.

82 F. Ju and Y. Hu, Removal of EDTA-chelated copper from aqueous solution by interior microelectrolysis, *Sep. Purif. Technol.*, 2011, **78**, 33–41.

83 O. Gylienė, J. Aikaitė and O. Nivinskienė, Recovery of EDTA from complex solution using Cu(II) as precipitant and Cu (II) subsequent removal by electrolysis, *J. Hazard. Mater.*, 2004, **B116**, 119–124.

84 Y. Yang, C. Gao, B. Li, L. Xu and L. Duan, A rhodamine-based colorimetric and reversible fluorescent chemosensor for selectively detection of Cu2+ and Hg2+ ions, *Sens. Actuators, B*, 2014, **199**, 121–126.

85 S. Kliem, M. Kreutzbruck and C. Bonten, Review on the Biological Degradation of Polymers in Various Environments, *Materials*, 2020, **13**, 4586.

86 T. Kirsipuu, A. Zadorožnaja, J. Smirnova, M. Friedemann, T. Plitz, V. Tõugu and P. Palumaa, Copper(II)-binding equilibria in human blood, *Sci. Rep.*, 2020, **10**, 5686.

87 D. Fischer, Y. Li, B. Ahlenemyer, J. Krieglstein and T. Kissel, In vitro cytotoxicity testing of polycations: influence of polymer structure on cell viability andhemolysis, *Biomaterials*, 2003, **24**, 1121–1131.

88 Y. Ji, F. Dai and B. Zhou, Designing salicylaldehyde isonicotinoyl hydrazones as Cu(II) ionophores with tunable chelation and release of copper for hitting redox Achilles heel of cancer cells, *Free Radicals Biol. Med.*, 2018, **129**, 215–226.

89 S. Anbu, R. Ravishankaran, M. F. C. Da Guedes Silva, A. A. Karande and A. J. L. Pombeiro, Differentially selective chemosensor with fluorescence off-on responses on Cu(2+) and Zn(2+) ions in aqueous media and applications in pyrophosphate sensing, live cell imaging, and cytotoxicity, *Inorg. Chem.*, 2014, **53**, 6655–6664.